A Rapid Calibration Method for Registration and 3D Tracking of Ultrasound Images Using Spatial Localizer

Emad M. Boctor[a], Ameet Jain[a], Michael A. Choti[b], Russell H. Taylor[a], and Gabor Fichtinger[a]

[a] Center of Computer-Integrated Surgical Systems and Technologies,
[b] Dept. of Surgery and Oncology; Johns Hopkins University

ABSTRACT

Conventional freehand 3D ultrasound (US) is a complex process, involving calibration, scanning, processing, volume reconstruction, and visualization. Prior to calibration, a position sensor is attached to the probe for tagging each image with its position and orientation in space; then calibration process is performed to determine the spatial transformation of the scan plan with respect to the position sensor. Finding this transformation matrix is a critical, but often underrated task in US-guided surgery. The purpose of this study is to enhance previously known calibration methods by introducing a novel calibration fixture and process. The proposed phantom is inexpensive, easy to construct, easy to scan, while yielding more data points per image than previously known designs. The processing phase is semi-automated, allowing for fast processing of a massive amount of data, which in turn increases accuracy by reducing human errors.

Keywords: 3D ultrasound, calibration, tracking, and registration

1. INTRODUCTION

During the past two decades surgical procedures have witnessed a revolutionary change, nowadays referred to as Computer Integrated Surgery. Especially with the introduction of various imaging modalities, like Magnetic Resonance Imaging (MRI), Computer Tomography (CT), and Ultrasound (US), surgical procedures have seen advancement in all stages, pre-, post-, and –intra-operative alike. True 3D imaging modalities, like MRI and CT, are extremely potent in terms of their rendering capabilities, but are cumbersome to use for intra-operative procedures, mainly due to obstructive hardware and imaging latency. Ultrasound, however, has been emerging as a widely popular image guidance modality, since it is real-time, convenient to use in the operating room, and readily inexpensive compared to CT and MRI.

Unfortunately, conventional ultrasound is predominantly a 2D imaging methodology. Significant amount of research has been conducted to convert this technology to provide the physicians with a 3D real-time visualization of the internal anatomy [1]. There are two basic methods to achieve this. The first, an intrinsically 3D method, is to either employ a fixed two-dimensional array transducer or a uniformly moving single array of sensors. This approach is somewhat limited, because scanning range is constrained by the hardware, which is quite often rather bulky. The second technique, an indirectly 3D method, is to let the surgeon manually acquire spatially co-registered 2D image slices, compound those into a contiguous 3D volume [2], then refresh the volume with real-time slices. This approach is highly applicable to tracking invasive surgical tools and compensating for organ motion. Significant research has been geared towards the more generally useable second method. We also present a companion paper in this subject at this conference, related to ablative liver therapy [3]. The quality and speed of volumetric compounding greatly depends on how well spaced and controlled the individual slices are, which can be greatly enhanced by robotic assistance [4][5]. A common way to co-register the individual 2D ultrasound slices is by tracking the imaging probe with magnetic or optical tracker. In this case, a fixed transformation between the US

Medical Imaging 2003: Ultrasonic Imaging and Signal Processing,
William F. Walker, Michael F. Insana, Editors, Proceedings of SPIE
Vol. 5035 (2003) © 2003 SPIE · 1605-7422/03/$15.00

beam and the tracker needs to be determined, so that arbitrary image pixels can be referenced in a global frame. Obtaining this fixed transformation is referred to as "ultrasound calibration". After calibration, a 3D volume is reconstructed by some surface- or voxel-based method, and then the data is visualized with some appropriate combination of surface extraction [6], volume rendering, re-slicing, panoramic viewing, or multi-planar techniques. Apparently, the accuracy of calibration greatly influences the quality of the reconstructed volume and visualization, through these the accuracy and realty of surgical planning and monitoring.

A widely popular way of calibration is imaging a precisely machined phantom of a priori known geometric properties. These properties are then identified in the images and their volumetric reconstruction is formulated in a mathematical framework that contains free variables for the unknown transformation. Then solving for the unknown variables provides us with the calibration parameters. There is error associated with each stage of the process (phantom fabrication, image acquisition, spatial co-registration, image processing, formulation, and numerical optimization solution), the combined total error of which may easily amount to a prohibitively large degree.

Most existing publications related to 3D ultrasound are concerned with volume measurements, reconstruction issues, image compounding, and accuracy of US scanning, while they treat calibration as a marginal necessity to achieve their main objective. Only few papers have been devoted solely to the investigation of probe calibration [7,8,9], while existing calibration methods critically need improvement in accuracy, ease of use, and performance time, and some of them need precise manufacturing of phantoms.

This paper focuses on enhancing the current methodology by introducing a novel calibration hardware, the Hopkins phantom and the multisided tank, with an associated mathematical framework. In contrast to prior methods, the Hopkins phantom is inexpensive, easy to construct and scan, yields significantly more data points per image than previously known designs, and easily to automate. We review the existing calibration methods (Cross-wire, Three-wires, and Single-wall) in terms of their physical design, achievable accuracy, number of images required, and the potential of full automation. The discussion continues with the Hopkins phantom and general mathematical framework used to solve the problem, and then we describe experimental validation and results.

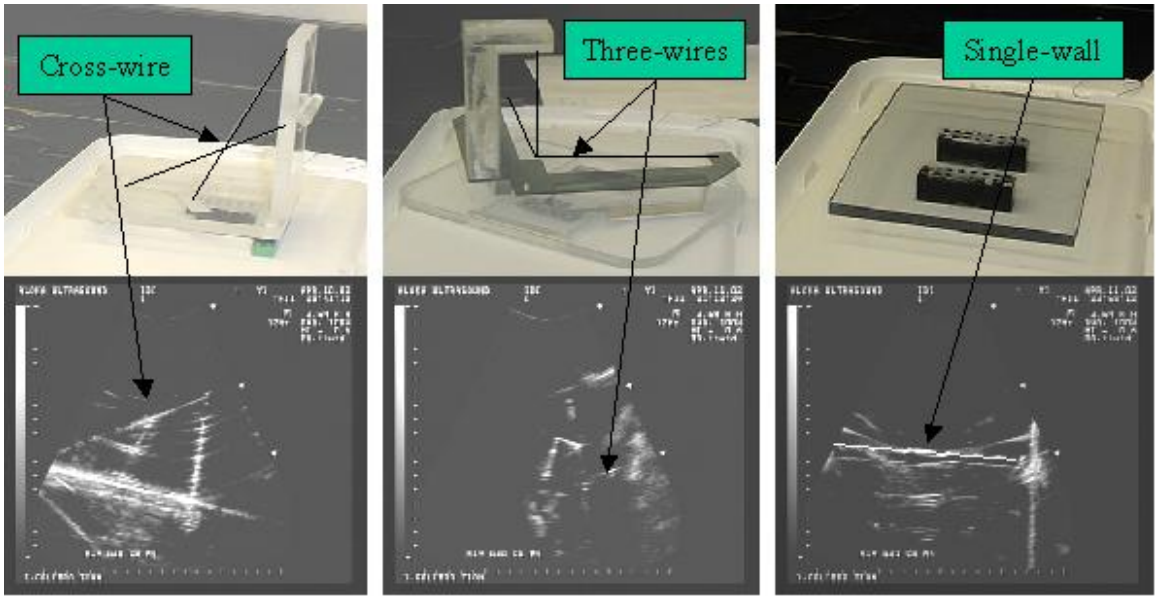

Figure 1: Calibration Phantoms and their corresponding US images; Left: Cross-wire phantom. Middle: Three-wires phantom, and Right: Single-wall phantom

1.1 Existing phantom-based calibration methods

Figure 1 shows three classic calibration phantoms that can be placed inside any tank for scanning from the top of the tank. The Cross-wire method [8] (Figure 2, left) is based on scanning the intersection of two crossing wires or some small object, like a bead or a pinhead. The target is suspended in water bath, it is scanned from different directions, and then crossing point (or pinhead) is detected manually in each image afterwards. The accuracy of this method depends, to a large degree, on the accuracy of the manual detection in the images. Each image provides only one data point that is extremely laborious to determine manually. The process is hard to automate because it is difficult to differentiate a single target is extremely from imaging artifacts.

The Three-wire phantom [7,8] (Figure 2, middle) involves scanning three wires submerged in a water bath and crossed in such a way that they constitute an orthogonal coordinate system. Like the Cross-wire technique, the wires here also need to be marked manually. The accuracy of this method also depends on whether the wires are precisely orthogonal and whether they are truly straight. The advantage of this method over the Cross-wire method is mainly that it is easier to scan the length of the wire than to keep the image focused at single point, while scanning from multiple directions.

The Single-wall method [8] (Figure 2, right), as its name suggests, features a planar surface immersed in water bath. This plane is viewed from various directions in the US images, each of which contains lines that lay in the plane. One problem with this method is that specular reflection causes low returning intensity at oblique scan angles. Furthermore, it is difficult to determine the true position of the floor in the images, solely based on reflected signal intensity. This is due to the strong reverberations from the bottom, which appear like a "comet tail" in the reflected intensity signal. The Cambridge phantom method, essentially, is an enhanced version of the Single-wall method. It overcomes both previously mentioned problems, but introduces dependencies on a precision-made phantom and clamp that is custom made for every different US probe.

1.2 Theory and mathematical framework

Figure 2 explains the mathematical framework of the calibration process, including the catenation of transformations between the coordinate frames. Our goal is to calculate ${}^{R}T_{P}$ transformation matrix between pixel frame P and receiver frame R. The calculation needs to be as accurate as possible, ideally, within the order of error of the tracker. Knowing this unknown transformation matrix would allow us to place every image pixel in the construction coordinate system, which can be affixed to the operation room or patient's body, conveniently.

The calibration phantom helps us determining the unknown transformation by providing fixed points in space, which appear clearly in the ultrasound images and they can be localized in the construction frame at the same time. There are three frame transformations: (1) ${}^{R}T_{P}$ matrix between the pixel frame and receiver frame, (2) ${}^{T}T_{R}$ matrix between receiver frame R and transmitter frame T, and (3) ${}^{C}T_{T}$ matrix between transmitter frame and construction frame. The equation involves 14 unknown variables: for ${}^{C}T_{T}$ and ${}^{R}T_{P}$, three translations and three rotations each, and the (S_x, S_y) scale factors for the (u,v) pixel coordinates. The ${}^{T}T_{R}$ matrix is known and this is the reading from the FOB tracker. Figure 3 shows the general form for of the unknown six degrees of freedom transformation matrices, as they are composed from the three rotations and three translation components. As the equations reflect, this problem is not a linear optimization that is usually straightforward to solve, but a non-linear optimization problem of large residual error type, which calls for the application of the Levenberg-Marquardt method.

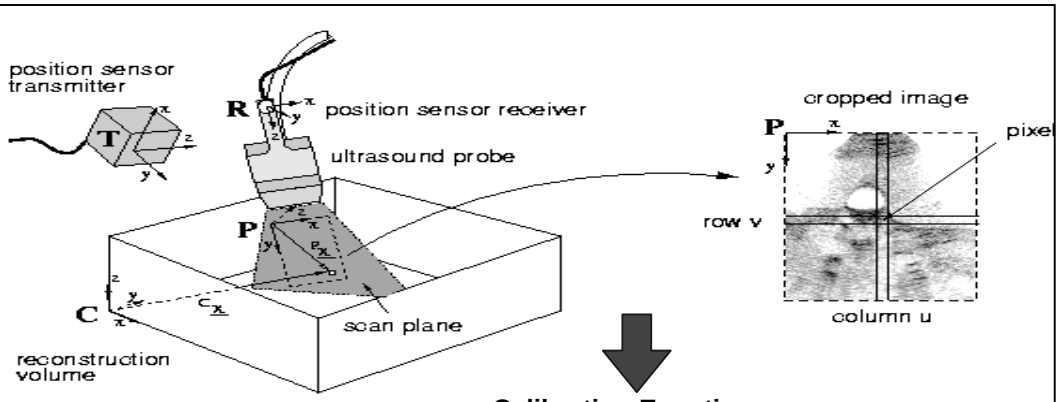

Calibration Equation

$$C_{\vec{x}} = {}^{C}T_{T}\,{}^{T}T_{R}\,{}^{R}T_{P}\,P_{\vec{x}}$$

$$P_{\vec{x}} = \begin{pmatrix} S_x u \\ S_y v \\ 0 \\ 1 \end{pmatrix}, C_{\vec{x}} = \begin{pmatrix} 0 \\ 0 \\ 0 \\ 1 \end{pmatrix}$$

Figure 2: The chain of transformations is from pixel frame P, to the receiver frame R, to transmitter frame T, and finally to construction frame C. The (u,v) pixel coordinates are multiplied by (S_x,S_y) scale factors. The resulting transformed point C_x has the (0,0,0) coordinate values [Cross-wire Phantom]. (Upper figure Courtesy of R. Prager)

$${}^{J}\mathbf{T}_{I}(x,y,z,\alpha,\beta,\gamma) = \begin{pmatrix} \cos\alpha\cos\beta & \cos\alpha\sin\beta\sin\gamma - \sin\alpha\cos\gamma & \cos\alpha\sin\beta\cos\gamma + \sin\alpha\sin\gamma & x \\ \sin\alpha\cos\beta & \sin\alpha\sin\beta\sin\gamma + \cos\alpha\cos\gamma & \sin\alpha\sin\beta\cos\gamma - \cos\alpha\sin\gamma & y \\ -\sin\beta & \cos\beta\sin\gamma & \cos\beta\cos\gamma & z \\ 0 & 0 & 0 & 1 \end{pmatrix}$$

$$\mathbf{0} = \mathbf{f}(\theta,\phi) \approx \mathbf{f}(\theta,\phi_j) + \frac{\partial \mathbf{f}(\theta,\phi_j)}{\partial \phi}(\phi - \phi_j)$$
$$\Rightarrow \Delta\mathbf{f} = \mathbf{J}(\phi - \phi_j) = \mathbf{J}\Delta\phi$$

$$\phi_{j+1} = \phi_j + (\mathbf{J}^T\mathbf{J} + \varepsilon\mathbf{I})^{-1}\mathbf{J}^T\Delta\mathbf{f}$$

Figure 3: The matrix on the top illustrates the general form of one of the six degrees of freedom transformation matrices (Three translations [x, y, and z] and Three rotations [α, β, and γ]). The equation in the bottom represents the Levenberg-Marquardt optimization method.

2. MATERIALS AND METHODS

2.1 Multisided tank and Hopkins phantom

For comparative analysis, we built a Cross-wire, a three-wire, and a single-wall phantom (Figure 1). Our experience showed that their designs and associated methods of data collection were not efficient and it was hard, if not impossible to automate the image segmentation phase of the calibration process. These observations inspired us to add two novel ideas to the methodology. The first innovation was to build a transparent plastic water tank, in which we can scan the submerged phantom not just from the top, but also from all four sides of the tank through rubber windows (Figure 4). The second innovation was to build a new phantom (called Hopkins phantom) that consists of two parallel plastic plates with parallel nylon lines stretched between the plates, in a pattern to form two orthogonal planes of a Cartesian coordinate system (Figure 5, left). The phantom is oriented in the multi-window tank in an oblique position, so that the structure can be scanned through two opposite windows and the top, with a plurality of nylon lines visible in each image (Figure 5, right). In every image, there is a set of parallel nylon lines near and far from the probe, which can enhance the accuracy and repeatability of calibration as Galloway pointed out [9]. The Hopkins phantom provides us with a large number of highly recognizable features collected from small number of images, allowing for automation of the task of image processing. Typically, only few images are sufficient for accurate calibration, which is a considerable reduction, compared to the typical 200 images with Cross-wire phantom or 400 images with three-wire phantoms [8]. In summary, the Hopkins phantom in conjunction with the multisided tank gives us the following advantages:

- Reduces the number of necessary images by a factor of 20, conservatively.
- Increases the number of data points in each image.
- Avoided the "beam width" problem that it is a constant problem with the Single-wall phantom.
- Easy to construct, and no special design requirements for any US probe used compared to the Cambridge phantom.
- The clarity of the calibration images enables easily automation of the calibration process.
- Images can be collected in a wide range of scanning motion.

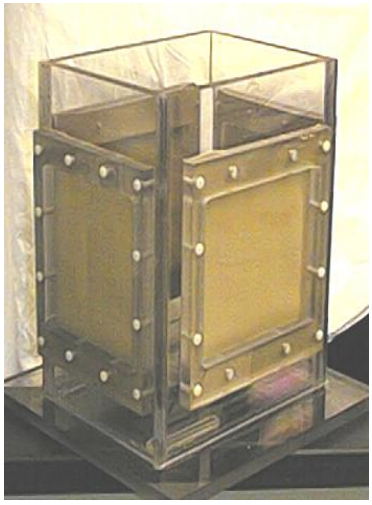

Figure 4: The Multisided tank is shown with five sides (top and four rubber windows). At the bottom, there is a piece of Lego to attach different phantoms.

Figure 5: The Hopkins phantom (left) and a typical image of it (right), illustrating the large number of data points that can be collected, in a potentially automated manner.

2.2 Setup and workflow

The experiment was conducted on a fixed laboratory bench. The Flock of Birds (FOB) transmitter was mounted at a height providing ample workspace of the sensor. Each of the phantoms was fixed inside the plastic tank by pieces from a Lego toy set. This was very important preventive measure, because any movement of the phantom relative to the transmitter during the experiment would render the whole calibration attempt void. For the same reason, tank was also fixed with respect to the transmitter.

The issue of speed of sound in water was carefully considered. The ultrasound machine does not let us input the speed of sound as a variable. Instead, it assumes an average velocity of sound for the human flesh, 1540m/s in our case, and then calculates its image pixel values accordingly. It is known that the speed of sound in water at room temperature is 1480m/s. Therefore, for precise calibration is necessary to dope the water in some fashion, so that the speed of sound in the tank would match the machine's hardwired constant. The simplest solution was to heat the water to 50° C, where the sound of speed in it is 1542m/s. Another constraint is that the glue holding the rubber windows on the tank loses strength at 59° C. Thus, the temperature had to be tightly regulated at around 50° C. We used the 112-point variant of the Bilaniuk and Wong formulas to obtain the speed of sound in pure water below, where c is the speed and T is the temperature in degrees of Celsius:

$$c = 1.40238742 \times 10^{3} + 5.03821344\,T - 5.80539349 \times 10^{-2}\,T^{2} + 3.32000870 \times 10^{-4}\,T^{3} - 1.44537900 \times 10^{-6}\,T^{4} + 2.99402365 \times 10^{-9}\,T^{5}$$

The preheated water was poured into the tank until the phantom was fully immersed in the water. The calibration process was performed twice with each phantom. First, the tank was placed adjacent to the transmitter, and then the calibration was repeated after the tank was moved farther away from the transmitter. When all the FOB readings are close to the transmitter, the absolute distances are small. Therefore, the percentage error of the tracking is relatively high, however the uncertainty (error) of the reading is low. Moreover, when the readings are all farther out, the percentage error must be smaller. However, the reading uncertainty is high. For comparative analysis, both datasets were taken.

In all sessions, the phantom was scanned from the top of the tank and from three of the four sides, while the fourth side of the tank faced conveniently the transmitter. (For example, for the Cross-wire and Hopkins phantoms, data was taken from three far sides and from top.) On each scanned side, 6-10 runs were performed at different angles between the probe and the tank. The US probe was moved slowly, in order to acquire a high number of scans in each run. Depending upon the type of phantom scanned, each run had the number of images ranging from 50 to 200. (In case of the Cross-wire phantom, an especially large number of images were needed, because the intersection of wires is not clearly visible in every image. Typically, we had to combine about 25 consecutive images to yield one reliable intersection point.)

2.3 Feature extraction

Once the large amount of raw data was collected, we needed to extract all useful information from it. With each frame an FOB reading was also taken at that very instant and stored, thus providing us with time-stamped, spatially correlated ultrasound images. By careful examination of all these images, the points of interest were segmented out, the pixel coordinates were noted, and a link was created between the pixel values and the corresponding FOB reading. These bundles were collected in a single file and fed to the numerical optimization program later. For example, in the case of the Cross-wire phantom, over 4400 images were processed manually for usable wire intersection points. This phase alone took about over 100 person-hours to complete. In order to aid this tedious and inherently error-prone process, a semi-automated method was created to store and log automatically the feature points that were selected manually upon a mouse click. This seemingly minor infrastructural enhancement significantly reduced the amount manual labor and work time, which in turn decreased the likelihood of human operator error. Ideally, we would like to achieve fully automated image processing, when all feature points are segmented out by software

without human intervention. In this approach, one would apply chain of filters to remove speckle and other artifacts as much as possible, and then geometric constraints would guide the segmenter to the true feature points. Unfortunately, the Cross-wire, Three-wire, and Single-wall phantoms do not allow for automated image processing, because the simple geometry of the phantom does not provide sufficient constraint for the feature tracker. Taking the crosswire image as an example (Figure 1, left), the feature doesn't have consistent echogenicity. This happened mainly because of the beam width effect. In other words, the appearance (echogenicity) of the crosswire depends on many parameters, as US power, time gain control (TGC) settings, depth, US probe type, lateral resolution, axial resolution, and most importantly the beam width. If the crosswire happens to be in the middle of the beam width, this should give more confined echo compared to the case at the beam edges. So in order to over come this problem, the Hopkins phantom designed in a way so that each reflector would cross the width of the beam from side to side with any angle of insonation (Figure 6). This will form a brighter spot for each reflector, where the size of this spot depends mainly on the width of the beam (amount of focusing), and later resolution as a function of depth. Figure 6 shows the upper reflector produced small bright echo because we have a good focusing zone (small beam width), and usually better lateral resolution at the shallow depth. On the other hand, the lower reflector produced larger spot in the axial direction due to the larger beam width and in the lateral direction mainly because the poor lateral resolution at the far zone. This is one of the prominent features of the Hopkins phantom, that allows for fully automated feature extraction in a reliable and repeatable way.

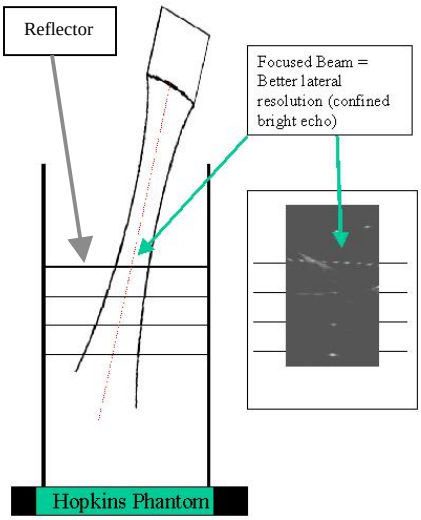

Figure 6: Shows how the Hopkins phantom is built to maintain well-

2.4 Verification on synthetic data

After the feature points were extracted from the images, the data was processed by running a numerical optimization algorithm to obtain the values of the unknown calibration matrix. As the problem is inherently non-linear in behavior with a large residual error, we decided to use the Levenberg-Marquadt method for non-linear least squares optimization. The code was written in Matlab, where the basic numerical functions were directly available. The authors generated synthetic input to check whether the optimization code was working correctly. They roughly estimated the value of ${}^{R}T_{P}$ and ${}^{C}T_{T}$ matrices with a common ruler. Then they extracted about 50 images from the pre-collected dataset with their corresponding ${}^{T}T_{R}$ transformation matrices. Utilizing ${}^{R}T_{P}$, ${}^{C}T_{T\backslash}$, and ${}^{T}T_{R}$ into the $P_x=[{}^{C}T_{T}\ {}^{T}T_{R}\ {}^{R}T_{P}]^{-1}C_x$ formula yielded a set of P_x points, the synthetic input data, in the image pixel frame. Using this input and the corresponding known ${}^{T}T_{R}$ matrices into the optimization code, resulting almost with the same ${}^{R}T_{P}$ and ${}^{C}T_{T}$ as those used for generating the synthetic data. The difference between these transformations was a negligible residual error left at the end of the optimization.

2.5 Initial guess

Non-linear optimization works the best if the algorithm starts from a good initial guess of the final solution, otherwise the algorithm may get trapped in a mirror solution or local minimum. Good initial estimate typically turns the optimization to low residual error problem, which then glides fast and smoothly to its true solution. Therefore, it is quite important to have a good initial guess for the 14 unknowns incorporated in ${}^{R}T_{P}$, ${}^{C}T_{T}$, S_x, and S_y.

The simplest case was S_x and S_y, because the approximate pixel scale factor was a priori known for the given Aloka SSD1400 US machine with a given set of scanning parameters, like the beam penetration depth. The value of the scale factors was 21 pixels per one centimeter uniformly in both directions, resulting 0.04878 cm^{-1} for both S_x and S_y.

The orientation of the FOB transmitter has no bearing on the experiment, so we were free to align it in a convenient way with respect to the construction frame, so that the ${}^{C}T_{T}$ would have a known rotational component or no rotation at all. Then the approximate values of the translational component of ${}^{C}T_{T}$ could be measured with a ruler or a calibrated tracked pointer.

There is a similarly simple way to estimate the six values in ${}^{R}T_{P}$ as well. Early in the construction phase of the system, we tried to align the FOB receiver symmetrically on the probe and without rotation. Therefore, the estimated ${}^{R}T_{P}$ has only three translation components and no rotation. With a ruler, we were able to measure the position of the FOB receiver from the ultrasound transducer, and then the position of the transducer with respect to the origin of the image pixel frame could be approximately determined from the images.

Another alternative to get an estimate of ${}^{R}T_{P}$ is shown in Figure 7. Vector 'a' is determined by using a calibrated tracked pointer to touch down the crosswire and record the reading. Then, capture any US image that contains the crosswire, and record the ${}^{T}T_{R}$ as shown in Figure 7. The (u,v) image pixel coordinates of the crosswire were read out from the image. From here, using S_x and S_y pixel scale factors, the (u,v) image pixel coordinates, and the plane normal, the P origin of the image pixel frame could be determined in the FOB transmitter frame. This resulted in a closed loop of transformations, from which obtaining ${}^{R}T_{P}$ was trivial.

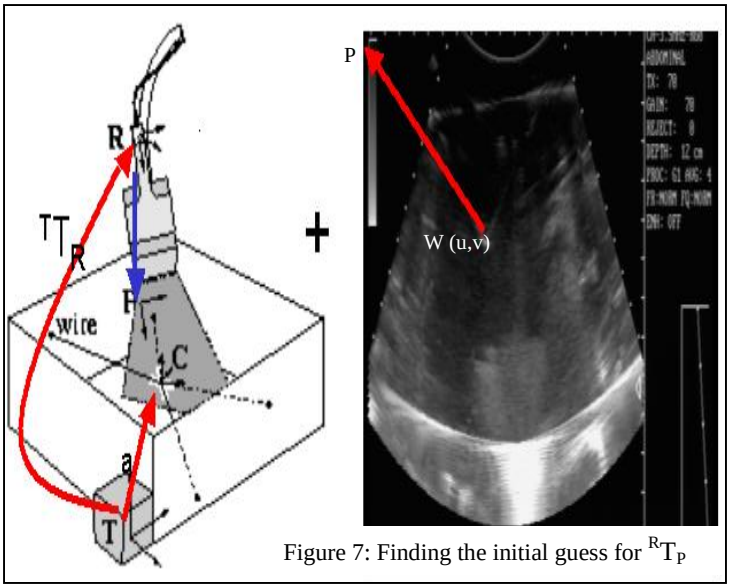

Figure 7: Finding the initial guess for ${}^{R}T_{P}$

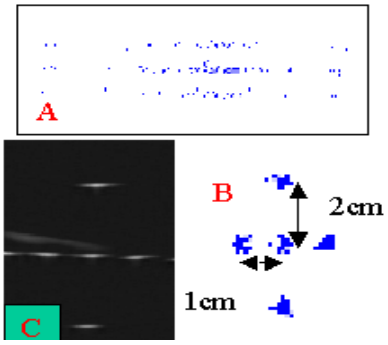

Figure 8: A: Points from Hopkins phantom extracted and placed in the construction-space. B: reconstruction of 5 reflectors in the Hopkins phantom's xy space. C: US image for these 5 reflectors.

3. RESULTS AND DISCUSSION

We tested two hypotheses. First, whether the multisided tank can provide significant improvements using with both current calibration methods and the new Hopkins phantom. The results were analyzed to measure the extent of improvements in terms of accuracy of the calibration process and/or the needed number of images to maintain that level of accuracy. The second hypothesis was to compare the Hopkins phantom and calibration method to the Cross-wire phantom that is one of the most commonly used methods. The Cross-

wire method is documented to be more accurate than the also popular Three-wires and the Single-wall methods.[8]

As it was previously mentioned, in order to analyze all these results and draw conclusions, accuracy and precision measures are needed. A straightforward way to measure the precision is to compute a number of calibration matrices with a given method and then to calculate descriptive statistics (mean, standard deviation, and range) for each variable in the calibration matrix. Ideally, the experiments should produce an identical calibration matrix in each repetition. This method of measuring the precision would require significant time, when repeating the same calibration method so many times. A more realistic measure of the precision measure is to map a fixed point in space from its position in the US image space to the receiver's space, using the derived calibration matrix, then to analyze the variability of this point in receiver space, in terms of mean, standard deviation and range of motions. Ideally, the point in receiver space should remain stationary with zero error, regardless to the position and insonation angles of the phantom. The Cross-wire phantom is used for this precision test by insonating the crosswire point (fixed point) from different views, using a previously obtained ${}^{R}T_{P}$ calibration matrix. We obtained ${}^{R}T_{P}$ from either the Hopkins or the Cross-wire phantom.

In each reconstruction, the crosswire point appeared as a cloud of at least 36 views (one crosswire point per view) collected from at least three sides of the tank, with 12 images per each side. The precision of reconstruction is then measured by evaluating the "tightness" of this cloud. The difference in position is calculated as observed from all possible combinations of two views out of all views, at least 630 combinations in each case, as follows:

$$\Delta^{T}\vec{x} = {}^{T}T_{R}^{view1}\,{}^{R}T_{P}\,{}^{P}\vec{x}^{view1} - {}^{T}T_{R}^{view2}\,{}^{R}T_{P}\,{}^{P}\vec{x}^{view2}, \quad \text{where} \tag{1}$$

$${}^{P}\vec{x}^{viewi} = \begin{pmatrix} s_u \times u^{viewi} \\ s_v \times v^{viewi} \\ 0 \\ 1 \end{pmatrix}$$

Where, S_u and S_v are the pixel ratios and $(u, v)^{viewi}$ is the crosswire position in the US space. Therefore, the magnitude of $\Delta^{T}\vec{x}$ reflects the precision of reconstructing the crosswire point. We have calculated this measure from all possible combinations from the 36 views.

Direct measuring of calibration accuracy is not as straightforward as measuring of precision, because the true calibration matrix is not known. One possible approach is to use synthetic sequences based on a known calibration and generate synthetic images with speckle noise for calibration[11]. This method checks the accuracy of calibration process compared to a known matrix, however, it is a simulated process and it doesn't use real US images that have different lateral and axial resolutions, beam width, side lobes, and speckle noise. In our approach, the Hopkins phantom plays a dual role, by serving as a calibration phantom and as a reconstruction accuracy measurement tool at the same time. The reflectors in the Hopkins phantom are separated by 1cm in one axis and 2cm in the other axis with 0.01 mm machining accuracy. The idea is to scan these reflectors with different insonation angles from different sides of the tank, and then to reconstruct them in tracker space. The next step is to measure the inter-distances between these reflectors to see the extent of deviation from the trusted 1 cm and 2 cm values (Figure 8).

3.1 Results with the multisided tank

To quantify the suspected benefits of the multisided tank, we have conducted series of experiments on both the Hopkins and Cross-wire phantoms. For both, three different solutions have been extracted based on the following datasets:

(1) Topside only, including 227 points for Hopkins phantom and 36 points for Cross-wire phantom.

(2) All sides with three times the data acquired from single side, as shown in Figure 4, yielding 704 points for Hopkins phantom and 119 points for Cross-wire phantom.

(3) All sides with the same number of data points as the single topside case.

Table 1 shows the resulting calibration matrices using both phantoms for above listed acquisition scenarios. The lower portion of the table discusses the reconstruction accuracy analysis that we conducted on

	Hopkins phantom				**Cross-wire phantom**		
Unknowns	Topside (n=227)	All sides (n=220)	All sides (n=230)	All sides (n=704)	Top side (n=36)	All sides (n=36)	All sides (n=119)
X (cm)	9.3387	9.4771	9.6347	9.7104	9.8440	9.4190	9.5385
Y (cm)	13.0277	12.6659	12.6267	12.9159	12.6467	13.1486	12.8696
Z (cm)	12.5079	11.7709	11.3023	11.4596	11.1253	11.1541	10.8402
α (rad)	-1.6505	-1.6374	-1.6465	-1.6516	-1.6614	-1.6598	-1.6572
β (rad)	0.0883	-0.0387	-0.0022	-0.0105	0.0255	-0.0127	0.0018
γ (rad)	0.0109	0.0010	0.0181	0.0190	0.0628	0.0025	0.0514
$S_x$mm/pxl	0.0480	0.0479	0.0476	0.0482	0.0473	0.0492	0.0483
$S_y$mm/pxl	0.0476	0.0479	0.0477	0.0479	0.0471	0.0496	0.0488

Reconstruction accuracy analysis applied with 1cm and 2cm inter-distance reflectors														
	1cm	2cm	1cm	2cm	1cm	2cm	1cm	2cm	1cm	2cm	1cm	2cm	1cm	2cm
Mean mm	-1.38	-0.40	-0.279	-0.184	-0.185	-0.083	-0.200	-0.259	-0.41	-0.041	-0.473	-0.835	-0.325	-0.494
STD mm	3.496	5.215	1.7847	2.0772	1.7631	1.9306	1.6790	1.5829	3.2755	3.0709	2.1697	1.6488	2.2412	1.7320
Min mm	6.804	10.46	5.7621	5.6484	3.7141	5.3666	4.6066	4.6066	6.5533	7.9437	4.9050	3.5693	5.5141	4.1137
Max mm	-10.8	-10.6	-6.602	-6.194	-5.764	-6.863	-5.360	-5.179	-10.63	-10.51	-6.616	-6.138	-6.676	-6.999

Table 1: Multisided tank analysis. The upper table shows estimated calibration matrices and pixel ratios by Hopkins and Cross-wire methods under different trials. These trails are based on spatial coverage of scanning (top side vs. multiple sides). The lower table shows the error statistics with the 1.0 and 2.0 cm inter-distance reflectors in the Hopkins phantom (Figure 8).

every calibration matrix. The table includes numbers for the reconstruction accuracy, with mean value, standard deviation and min-max range. The mean value is the average difference between the true (1cm and 2 cm as shown in Figure 8) and the calculated inter-distances of the two reflectors taken from all possible views, thus representing the amount of misregistration in reconstruction space. The standard deviation represents the uncertainty of reconstruction accuracy. Observing all, but especially the mean and STD values, it is obvious that calibration with the multisided tank substantially enhances the accuracy of calibration, regardless to whether the Hopkins and Cross-wire phantom is used. For example, the standard deviation in the Hopkins phantom dropped from 5.2 to 1.5 between the "Topside N=227 points" and "All-sides N=704 points" cases. Using the same number of data points, but collected evenly from multiple sides of tank produces very good and reliable results. Taking the Cross-wire phantom as an example with 1-cm

reflector distance, the STD is in the order of 2.1-2.2 mm using all sides of the tank, as opposed to 3.2 mm using for the topside only, and even regardless to dropping the number of points from 119 to 36.

An average image of the Hopkins phantom yields 20 data points. This means that a highly reasonable set of 220 points could be collected from just 10-12 images, which is sufficient to produce a very accurate calibration matrix, if the images are collected from all sides of the tank. Altogether, using the Hopkins phantom with the multisided tank, just 3-4 images collected from each side can produce a very accurate calibration matrix. Furthermore, the optimization framework remains stable with even fewer images and data points. For example, the condition number of the Jacobian matrix in Levenberg-Marquardt method near to the solution remains bounded at about 150 while using only 80 points collected from all side combined.

3.2 Comparison of the Hopkins and Cross-wire phantoms

We have applied two different analytical techniques to compare the accuracy of the Hopkins and Cross-wire phantoms. These techniques are with precision accuracy of the reconstruction accuracy, as we alluded to in the beginning of the "Result and Discussion" section. For normalization, we used manual feature extraction for both methods, and acquired multisided data for both phantoms.

	Trial #1				Trial #2			
	Hopkins		Cross-wire		Hopkins		Cross-wire	
	1cm	2cm	1cm	2cm	1cm	2cm	1cm	2cm
Mean(mm)	-0.1472	0.0041	-0.1726	-0.1038	-0.2000	-0.2585	-0.3102	-0.4083
STD (mm)	1.0806	2.1857	1.2437	1.9010	1.6790	1.5829	2.1764	1.7811
Min (mm)	3.7318	8.5480	5.3191	5.5081	4.6066	4.6066	5.0594	4.4829
Max (mm)	-3.2152	-5.1998	-4.4075	-6.3755	-5.3604	-5.1786	-6.8606	-7.2443

Table 2: Comparison between the Hopkins phantom and the Cross-wire phantom based on reconstruction accuracy measures

	Trial #1		Trial #2	
	Hopkins	Cross-wire	Hopkins	Cross-wire
Mean(mm)	0.8376	0.7732	0.6053	0.4681
STD (mm)	0.3950	0.3451	0.2828	0.2260
Min (mm)	0.0287	0.0332	0.0180	0.0195
Max (mm)	2.4228	2.0373	1.7882	1.3744

Table 3: Comparison between the Hopkins and Cross-wire phantoms, based on reconstruction precision measures.

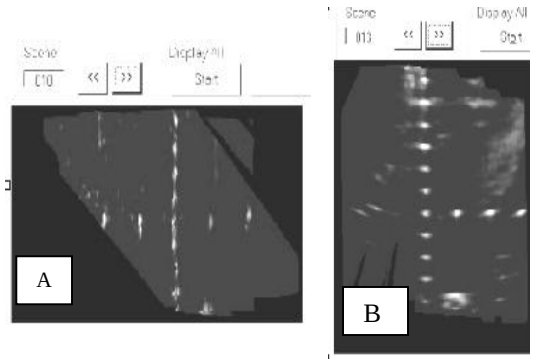

Figure 9: "A" shows the reconstruction of the Hopkins phantom by using the calibration matrix of the Cross-wire method. "B" shows the reconstruction based on Hopkins calibration parameters. It is obvious that Hopkins method leads to more reconstruction accuracy as it is shown in Table1 as well.

Table 2 shows two reconstruction accuracy analysis trials for Hopkins and Cross-wire phantoms, both indicating the superiority of the Hopkins method, in terms of the mean error of reconstruction accuracy,

while the standard deviation is almost the same for both. Table 3 shows the results of reconstruction precision experiments and illustrates that both phantoms are in the same order of precision. Figure 9 is a visual realization of reconstruction accuracy tests. It can be seen clearly that Hopkins method reconstructs the acquired data and registers them in the construction space more accurately.

4. CONCLUSIONS

Our experiences proved that the introduction of a multisided tank improves the speed and accuracy of the calibration process in several aspects. The new Hopkins phantom provides a large number of data points from only a few images. It is sufficient to collect just 10-12 images and the calibration matrix can be obtained accurately, even without a good initial guess. Due to its design and construction, the Hopkins phantom allows for static tracking. The content and quality of images allow for fully automated calibration.

The future work of this project is to continue further analysis for both Hopkins method and the multisided tank. In the hope to answer, the question of what is exactly the minimum number of images and from which directions could meet certain accepted level of accuracy. Furthermore, part of the future work is to test these results in an integrated application, using 3D US system as a guiding tool for interventional surgery[3].

ACKNOWLEDGEMENTS

The authors gratefully acknowledge the support and help offered by Mr. John Walsh (ALOKA Inc.) by providing the SSD1400 US equipment. We also thank Ankur Kapoor, Greg Fisher and Anton Deguet for their advices and help. This work was supported by the National Science Foundation under Engineering Research Center grant #EEC 9731478.

REFERENCES

1. Thomas N., Dolores H. P., “Three-Dimensional Ultrasound Imaging”, Ultrasound in Med. & Biol. Vol. 24, No. 9, pp. 1243-1270, 1998
2. Emad Boctor, A. Saad, Dar-Jen Chang. PC-Based system for calibration, Reconstruction, Processing and Visualization of 3D Ultrasound Data Based on a Magnetic-Field Position and Orientation Sensing System, in ICCS, Lecture Notes in Computer Science, Springer Verlag, 2001
3. E. Boctor, G. Fichtinger, R. H. Taylor, M. A. Choti, Johns Hopkins Univ. “Tracked 3D ultrasound in radio-frequency liver ablation” SPIE Medical Imaging 15-20 Feb 2003, San Diego, California USA.
4. E. Boctor, R. H. Taylor, G. Fichtinger, M. A. Choti, Johns Hopkins Univ. “Robotically assisted intraoperative ultrasound with application to ablative therapy of liver cancer” SPIE Medical Imaging 15-20 Feb 2003, San Diego, California USA.
5. S.E. Salcudean et al. “Robot Assisted Diagnostic Ultrasound – Design and Feasibility Experiments”, in MICCAI, Lecture Notes in Computer Science, pp-1062-1071, Springer, 1999.
6. Emad M. Boctor, A. A. Saad and Prof Abo Bakr Youssef (PhD/MD), “Estimation of prostate volume by using 3D ultrasound imagery system”, presented in the International Congress of Ultrasonography in collaboration with Hannover University-Germany, April 10-12th, 1998 Cairo, Egypt.
7. J. Carr, “Surface reconstruction in 3D medical imaging,” Ph.D. thesis, University of Canterbury, Christchurch, New Zealand, 1996.
8. R.W. Prager, R. Rohling, A. Gee, and Berman L. “Rapid calibration for 3D freehand ultrasound,” Ultrasound in Medicine and Biology, vol. 24, no. 6, pp. 855-869, 1998.
9. Diane M. Muratore, Robert L. Galloway, Jr., “Beam Calibration without a Phantom for Creating a 3D Free-hand Ultrasound System” Ultrasound in Med. & Biol., Volume 27, No. 11, pp1557-1566, 2001
10. Niko Pagoulatos, David R. Haynor and Yongmin Kim, “A Fast Calibration Method for 3D Tracking of Ultrasound Images Using a Spatial Localizer” Ultrasound in Med. & Biol., Volume 27, No. 9, pp 1219-1229, 2001.
11. Francois Rousseau, Pierre Hellier and Christian Barillot, “A Fully Automatic Calibration Procedure for Freehand 3D Ultrasound”, IEEE ISBI Conference, July 2002.